IEEE Access
Multidisciplinary | Rapid Review | Open Access Journal

Received December 16, 2018, accepted January 18, 2019, date of publication January 30, 2019, date of current version February 20, 2019.

Digital Object Identifier 10.1109/ACCESS.2019.2896309

A Parameter-Free Linear Sampling Method

LEI LIU[1] AND GUANZHONG HU[2]

[1]College of Electrical Engineering, Zhejiang University, Hangzhou 310027, China
[2]School of Electrical Engineering and Mechano-Electronic Engineering, Xuchang University, Xuchang 461000, China

Corresponding author: Guanzhong Hu (gz_hu@yahoo.com)

This work was supported in part by the National Natural Science Foundation of China under Grant 51741702, and in part by the Fundamental Research Funds for the Central Universities under Grant 110401∗172210181.

ABSTRACT An inverse electromagnetic scattering problem is to determine the support of a scatterer from the scattered field or its far-field pattern. Characterized by ill-posedness and nonlinearity, the solution to this problem has difficulty in numerical implementation. The linear sampling method (LSM) is known to be a simple and computational efficient approach to retrieve the support of scatterers using multistatic scattered field data. However, the recovered profile is always misleading, owing to the lack of robust edge detecting as well as the frequency dependence of the LSM. In this paper, free from *a priori* information pertaining to the geometry to be inspected, the upper and lower bounds of the profile of scatterers are pursued. All the required data are generated by the LSM, which are utilized to construct a surface presentation of the indicator function in terms of moving least square approximation. The bounds are extracted from the curvature of such surface. Moreover, with the aid of the retrieved support of the scatterers, the sensible frequency limit of the incident electromagnetic wave is estimated *a posteriori*. In the end, the experimental results validate the proposed method.

INDEX TERMS Frequency dependence, linear sampling method, moving least square approximation

I. INTRODUCTION

The electromagnetic scattering inverse problem is concerned with the reconstruction of the shape and the electromagnetic parameters of unknown targets given scattered field or its far-field pattern. Newton-type iterative method [1], [2] and regularization tools are employed extensively to solve this problem. Although these techniques were successfully applied in certain scenarios, as a typical nonlinear and ill-posed problem, it is numerically expensive and relies on a priori information about the scatterer (size, physical parameters, and boundary conditions, etc.). To overcome these difficulties, methods with less a priori information and numerical burdens are sought. At this point of view, the linear sampling method (LSM) [3] is a promising technique, which could find the support of the scatterer with very limited a priori information, and involves only the solution of linear ill-posed problems.

However, all these merits are obtained at the cost of losing accuracy: the LSM is a qualitative method that only the support of the scatterers and partial information on the material properties can be retrieved. The combination of iterative methods and the LSM is necessary to provide a promising solution. Another important problem of the LSM is of its ill-posedness. Although the regularization could promise a stable solution, the blowing-up numerical behavior of the LSM is relaxed. This results in a series of contours, and only one of them is optimal to approximate the profile of scatterers. To determine the optimal contour level, many approaches were proposed to provide the cut-off value associated with certain contour line. In the calibration method, the forward data of known scatterers, which assumes a similar size to the target to be inspected, are utilized to extract the best cut-off value [4]. Another similar approach assumes that a known object is near the scatterers to be identified. The cut-off value of the known object is employed to calibrate that of the unknown scatterers [5]. Both schemes are able to give satisfactory cut-off value in a simple and straightforward manner. Unfortunately, employment of appropriate calibration or reference objects is equivalent to a priori geometry information of the scatterers to be inspected. Aramini *et al.* [6] suggest a deformable model approach to adjust the contour based on the indicator itself. This edge detection is especially robust, but the minimizing is costly for a qualitative approach. We had better use the results generated by the LSM as an initial guess for iterative methods. All these available approaches

The associate editor coordinating the review of this manuscript and approving it for publication was Lei Zhao.

are ad hoc approaches depending on the predefined parameters. To make matters worse, the behavior of the LSM is frequency dependent. The reconstruction of the support of scatterers is deteriorated when the frequency of the incident electromagnetic wave is too low or too high beyond certain limits [7]. It is still an unsolved problem to determine the optimal frequency range that best approximates the profile of the scatterers, although some rules of thumb and heuristic interpretations are proposed [8].

This paper addresses the aforementioned problems. Firstly, the results of the LSM are fitted to a response surface, and thus a geometric feature analysis is proposed to find the profile of unknown targets. As a result, using a single-frequency scattered field data, we can find the profile of the scatter to be inspected without further a priori information. To the best of our knowledge, there are still no simple strategies available to tell how to choose a cut-off value with such restricted data. Secondly, a relationship between the frequency of the incident wave and the residuals of the regularized far field equation, combined with the retrieved support of the scatterer, is used to estimate the sensible upper frequency limit.

II. THE LSM BASICS

Without loss of generality, we consider the two-dimensional case in the following sections. Let $\Omega \subset R^2$ be a space region containing the scatterer D to be inspected. The scatterer is made of perfect electric conductor, illuminated by a plane wave impinging from directions

$$\hat{\boldsymbol{d}} = \cos\theta\hat{\boldsymbol{x}} + \sin\theta\hat{\boldsymbol{y}} \tag{1}$$

being $\hat{\boldsymbol{x}}$, $\hat{\boldsymbol{y}}$ the Cartesian unit vectors, $\theta \in [0, 2\pi)$. Accordingly, we have the far-field pattern $\boldsymbol{E}_\infty(\hat{\boldsymbol{r}}, \hat{\boldsymbol{d}})$, where $\hat{\boldsymbol{r}}$ denotes the observation direction. The description of LSM begins with the definition of the so called far-field equation, which reads:

$$\oint_C \boldsymbol{E}_\infty(\hat{\boldsymbol{r}}, \hat{\boldsymbol{d}}) g(\boldsymbol{x}, \hat{\boldsymbol{d}}) \cdot ds(\hat{\boldsymbol{d}}) = \boldsymbol{E}^e_\infty(\hat{\boldsymbol{r}}, \boldsymbol{x}) \tag{2}$$

where $\boldsymbol{x} = (x, y) \in \Omega$. C denotes a unit circle contour as the integral path, $g(\boldsymbol{x}, \hat{\boldsymbol{d}})$ is an unknown function of each sampling point, which is used to define the indicator function, and

$$\boldsymbol{E}^e_\infty(\boldsymbol{r}, \boldsymbol{x}) = \frac{e^{j\pi/4}}{\sqrt{8\pi k}} e^{-jk\hat{\boldsymbol{r}}\cdot\boldsymbol{x}} \tag{3}$$

is the far-field pattern of the fundamental solution of the Helmholtz equation. In this paper, (3) and all other formulae obey $e^{-j\omega t}$ convention. Based on above presumptions, the following important theorem holds true:

Theorem: (i) if $\boldsymbol{x} \in D$ and for all $\varepsilon > 0$, there exists $g(\boldsymbol{x}, \hat{\boldsymbol{d}})$ such that

$$\left\| \oint_C \boldsymbol{E}_\infty(\hat{\boldsymbol{r}}, \hat{\boldsymbol{d}}) g(\boldsymbol{x}, \hat{\boldsymbol{d}}) \cdot ds(\hat{\boldsymbol{d}}) - \boldsymbol{E}^e_\infty(\hat{\boldsymbol{r}}, \boldsymbol{x}) \right\| < \varepsilon \tag{4}$$

and

$$\lim_{\boldsymbol{x} \to \partial D} \left\| g(\boldsymbol{x}, \hat{\boldsymbol{d}}) \right\| = \infty \tag{5}$$

(ii) For $\boldsymbol{x} \notin D$ and for all $\varepsilon > 0$, any feasible $g(\boldsymbol{x}, \hat{\boldsymbol{d}})$ satisfying the inequality (4) is such that

$$\lim_{\varepsilon \to 0} \left\| g(\boldsymbol{x}, \hat{\boldsymbol{d}}) \right\| = \infty \tag{6}$$

This theorem implicates that there exists an approximated solution of the far-field equation (2), whose norm blows up near the boundary of the scatterers and remains arbitrarily large outside of them. In the LSM, these singularities are used to construct indicator functions so that the support of the scatterers can be characterized. $\mathrm{I}(g(\boldsymbol{x}, \hat{\boldsymbol{d}})) = 1/||g(\boldsymbol{x}, \hat{\boldsymbol{d}}))||$ or $\mathrm{I}(g(\boldsymbol{x}, \hat{\boldsymbol{d}})) = \lg||g(\boldsymbol{x}, \hat{\boldsymbol{d}}))||$ are prevalent candidates for the indicator function. A certain contour line of the indicator functions is utilized to represent the profile of the scatterer. Noted that to make the numerical implementation of the LSM possible, it is necessary to relax the aforementioned singularities.

III. THE PROPOSED POSTPROCESSING

No matter which regularization is applied, the corresponding solution definitely eliminates the singularity near the profile of the scatterers owing to the smoothing effect of the regularization. This leads to ambiguities of the edge detection using the indicator function, which deteriorates the accuracy of the retrieval of the support of the unknown scatterers.

A. THE GEOMETRIC FEATURE BASED EDGE DETECTION METHOD

Although it is common to extract information from the values of an indicator function over a sampling grid, more attributes are endowed with the indicator function. In effect, an indicator function, with fixed $\hat{\boldsymbol{d}}$, could be regarded as a surface. Therefore, it is possible, with the aid of some geometric interpretation, to recover more information on the unknown scatterers. One of the most important geometric features of a surface is its curvature.

Curvature is a two-dimensional property of a curve. It is originally defined as the rate of change of direction for a particular point on the curve. Intuitively speaking, the curvature describes how bent a curve is at a particular point on the curve. This two-dimensional concept can be generalized to three-dimensions (or even higher dimensions). There is a family of curves through a particular point on the surface. An infinite number of curvatures, which are orthogonal to the surface, can thus be extracted. These are so-called normal curvatures, and they can be combined in different ways in revealing various properties of the relevant surface. Given any point on the surface, there exist the largest absolute normal curvature K_{max} and the smallest absolute normal curvature K_{min}, respectively, from the infinite number of normal curvatures. K_{max} and K_{min} are referred to as the principal curvatures and they are orthogonal to each other. K_{max} proves to be very effective at delimiting fault geometries [8].

As aforementioned argument, the regularized surface of the indicator function is a smoothed version of the original one. As depicted in Fig. 1 (*a*), this effect is described by the

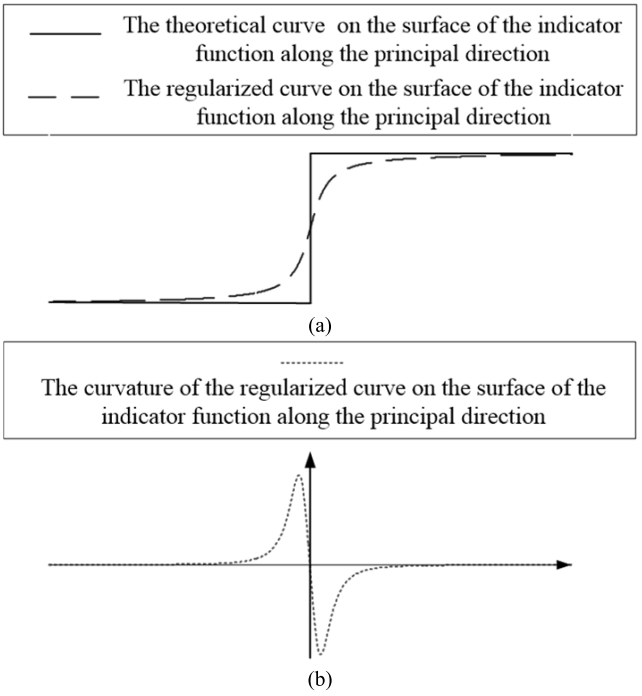

FIGURE 1. The comparison between regularized curve on the surface of the indicator function along the principal direction and its theoretical counterpart. (a), and the curvature of the regularized curve (b), i.e., maximum curvature.

differences between the theoretical curve and the regularized curve, given by the intersection of the surface of the indicator function and the plane of maximum curvature. Concerning on the curvature of the curve in Fig. 1 (*a*), artificial curvatures over the singularities claimed by the theorem in section II are introduced, with high positive curvature on the up-thrown side and high negative curvature on the down-thrown side, as shown in Fig. 1 (*b*).

It is clear that such artificial curvatures provide the information of the upper and lower bounds of the location of singularities, i.e., the profile of the scatterer. Following this line of thinking, the average curvature can be defined on every contour line, which is computed as follows

$$K_a = \int_\Gamma K_{\max} dl \Big/ \int_\Gamma dl \tag{7}$$

where K_{max} is the maximum curvature at the points along the contour line Γ. Once the contour lines with a local optimum of K_a are found, they can be regarded as the upper and lower bounds of the scatterer. To evaluate (7), it is necessary to compute K_{max} on the surface of the indicator function using the sampling points over a grid, which is detailed as follows.

B. THE COMPUTATION OF THE CURVATURE OVER THE SAMPLING GRID

Moving least squares approximation is an extension of the well-known least squares to fit a surface to a given scattered data points [9], [10]. These least squares are spatially weighted so that the region around the reconstructed point is biased. In this way, the basis functions are locally supported. This method works very well for interpolation, smoothing and derivative approximations, which is well suited for the computation involved in this paper

Given certain direction $\hat{\boldsymbol{d}}$, let the indicator function is approximated by a least squares approximation

$$I(g(\boldsymbol{x}, \hat{\boldsymbol{d}})) \approx \sum_{i=1}^{M} c_i B_i(\boldsymbol{x}) \tag{8}$$

where c_i are the undetermined coefficients associated with the basis functions $B_i(\boldsymbol{x})$, which are usually linearly independent polynomials, such as 1, x, x^2, ...in one-dimensional case. Given the sampling pairs $\boldsymbol{x}_i$ and its corresponding indicator function $I(g(\boldsymbol{x}_i, \hat{\boldsymbol{d}}))$, $i = 1, \ldots, N$. The best fit of (8) is defined as

$$\arg\min \sum_{i=1}^{N} \left\| I(g(\boldsymbol{x}, \hat{\boldsymbol{d}})) - \sum_{j=1}^{M} c_j B_j(\boldsymbol{x}) \right\| w(\|\boldsymbol{x} - \boldsymbol{x}_i\|) \tag{9}$$

over all polynomials $B_j(\boldsymbol{x})$. $w(||\boldsymbol{x}-\boldsymbol{x}_i||)$ are non-negative local weight function, i.e, it decays fast as $||\boldsymbol{x} - \boldsymbol{x}_i|| \to \infty$. As a consequence, c_i are evaluated via the solving of the normal equations

$$\sum_{i=1}^{M} c_i [B_i(\boldsymbol{x}), B_j(\boldsymbol{x})]_{w(\boldsymbol{x})} = [I(g(\boldsymbol{x}, \hat{\boldsymbol{d}})), B_j(\boldsymbol{x})]_{w(\boldsymbol{x})} \tag{10}$$

anew whenever $\boldsymbol{x}$ is changed. where [,] is the inner product induced by $w(||\boldsymbol{x} - \boldsymbol{x}_i||)$.

Let the basis functions be quadratic polynomials, it is sufficient to evaluate the curvature of the response surface of the indicator function obtained by the moving least squares approximation. In this paper, the weight function $w(||\boldsymbol{x}-\boldsymbol{x}_i||)$ takes the form of splines as follows:

$$w(r) = \begin{cases} 2/3 - 4r^2 + 4r^3 & 0 < r \le 0.5 \\ 4/3 - 4r + 4r^2 - (4r^3)/3 & 0.5 < r \le 1 \\ 0 & 1 < r \end{cases} \tag{11}$$

where $r = ||\boldsymbol{x} - \boldsymbol{x}_i||/r_{max}$. and r_{max} is the base value that is several times the average distance between sampling points.

With the increase of the sampling points, the system of (10) is ill-posed. To circumvent this problem, the singular value decomposition is applied, i.e.,

$$([B_i(\boldsymbol{x}), B_j(\boldsymbol{x})]_{w(\boldsymbol{x})})_{ij} = USV^T \tag{12}$$

where S is an $n \times n$ diagonal matrix containing M singular values. If a singular value is smaller than a predefined threshold, its corresponding row and column of S, as well as the corresponding columns of U and V are removed. This leads to a well-posed and reduced system.

Since the reconstructed surface of the indicator function is continuous, the maximum curvature of any specific point can be calculated. The direct maximum of the normal curvatures is obviously out of reach. Here, we first compute the mean curvature K_m and the Gaussian curvature K_g [13]:

$$K_m = (EN - 2FM + GL)/[2(EG - F^2)]$$
$$K_g = (LN - M^2)/(EG - F^2)$$

where

$$
\begin{aligned}
E &= 1 + (\partial I/\partial x)^2 \\
F &= 1 + (\partial I/\partial x)(\partial I/\partial y) \\
G &= 1 + (\partial I/\partial y)^2 \\
L &= (\partial^2 I/\partial x^2)/\sqrt{1 + (\partial I/\partial x)^2 + (\partial I/\partial y)^2} \\
M &= (\partial^2 I/\partial x \partial y)/\sqrt{1 + (\partial I/\partial x)^2 + (\partial I/\partial y)^2} \\
L &= (\partial^2 I/\partial y^2)/\sqrt{1 + (\partial I/\partial x)^2 + (\partial I/\partial y)^2}
\end{aligned}
$$

Since $B_i(\boldsymbol{x})$ are polynomials, the evaluation of $\partial I/\partial x$, $\partial I/\partial y$, $\partial^2 I/\partial x^2$, $\partial^2 I/\partial x \partial y$, and $\partial^2 I/\partial y^2$ are fairly easy. In terms of K_m and K_g, K_{max} can be easily deduced owing to the following identities:

$$K_m = \frac{K_{\max} + K_{\min}}{2} \tag{13}$$

$$K_g = K_{\max} K_{\min} \tag{14}$$

The resulting K_{max} is derived

$$K_{\max} = K_m + \sqrt{K_m^2 - K_g} \tag{15}$$

C. ALGORITHM DESCRIPTION

The foregoing formulations and arguments allow summarizing the main components of the proposed post-processing as follows:

Given the sampling of the indicator function over a grid in the region where D is sought.

(1) Reconstruct the response surface of the indicator function over the sampling points.

(2) Plot the contours of the indicator function with predefined levels.

(3) Evaluate (7) using numerical integrals, in which the maximum curvature is obtained by means of (13)-(15).

(4) Compare the results of (7) for all the contours; the contour with the maximum and the minimum values are regarded as the lower and the upper limit, respectively.

IV. FREQUENCY ESTIMATION

Although the behavior of the LSM is frequency dependent, a priori information is generally unavailable. The promising method of selecting the frequency of the incident electromagnetic wave is to estimate the optimal frequency range in terms of the initial reconstruction of the LSM.

In [14], a physical interpretation of the LSM is established based on the Poynting vector associated with the far-field equation. To prove the properties of the power flow lines, an inequality is deduced:

$$(\sqrt{2} - 1)\sqrt{\frac{\psi_\infty(z)}{8\pi k}} > \varepsilon \tag{16}$$

where $\psi_\propto(\boldsymbol{z})$ is the asymptotic angular width of the regular energy flow strip in the neighborhood of the sampling point $\boldsymbol{z}$. ε is the residual norm of the far-field equation corresponding to sampling point $\boldsymbol{z}$. k is the wave number of the incident electromagnetic wave. For detailed deviation we refer to [14]. The explicit computation of the bound (16) can be simplified for $\boldsymbol{z}$ belongs to the identified object. In this case, the behavior of the flow lines is radial with respect to z, and $\psi_\propto(z) = \pi$ given C^2-boundary of the identified profile. Rearranging (16), the bound is expressed as:

$$f < \frac{3 - 2\sqrt{2}}{16\pi\sqrt{\mu_B \varepsilon_B}} \frac{1}{\varepsilon^2} \tag{17}$$

where μ_B and ε_B are the permittivity and permeability of the background medium, respectively. (17) provides a natural upper limit of the sensible frequency f of the incident electromagnetic wave. If the frequency of the incident electromagnetic wave is adjustable, we could use this criterion to improve the resolution of the reconstructed shape.

V. NUMERICAL EXAMPLES

A. NUMERICAL IMPLEMENTATION OF THE LSM

For the sake of simplicity, we consider the two dimensional TM wave scatterings by different scatterers. In those numerical examples, the incident wave and scatterers are chosen in a priori: Plane waves impinge from N equally spaced directions as follows:

$$
\begin{aligned}
\hat{\boldsymbol{d}}_j &= \cos\theta_j \hat{\boldsymbol{x}} + \sin\theta_j \hat{\boldsymbol{y}} \\
\theta_j &= 2\pi j/N, \quad j = 1, \ldots, N
\end{aligned} \tag{18}
$$

Then the electric far field pattern $\boldsymbol{E}_\infty(\hat{\boldsymbol{d}}_\mathrm{i}, \hat{\boldsymbol{d}}_\mathrm{j})$ is computed by the method of moment. Random noise is injected to the computed pattern to avoid inverse crimes [12]:

$$E^\delta_{l,m}(\hat{\boldsymbol{d}}_i, \hat{\boldsymbol{d}}_j) = E_\infty(\hat{\boldsymbol{d}}_i, \hat{\boldsymbol{d}}_j)(1 + \delta\xi_{ij}) \tag{19}$$

where $\varepsilon = 0.01$ is the level of perturbation and ξ_{ij} is a uniformly distributed random number between -1 and $+1$.

For simplicity, we now approximate far field equation (2) using midpoint rule, which results in a matrix equation in the form of

$$\boldsymbol{A}^\delta g_z = b_z \tag{20}$$

where $g_{\boldsymbol{z}}$ is $g(\boldsymbol{z}, \hat{\boldsymbol{d}})$ for a sampling point $\boldsymbol{z}$, and

$$
\begin{aligned}
\boldsymbol{A}^\delta_{ij} &= E^\delta_{l,m}(\hat{\boldsymbol{d}}_i, \hat{\boldsymbol{d}}_j) \\
(b_z)_l &= \frac{N}{2\pi} E^e_\infty(d_l, z)
\end{aligned}
$$

Because (20) is highly ill-posed, Tikhonov regularization is used to approximate its solution by solving

$$(\alpha_z I + (\boldsymbol{A}^\delta)^* \boldsymbol{A}^\delta) g^\alpha_z = (\boldsymbol{A}^\delta)^* b_z \tag{21}$$

where $\alpha_{\boldsymbol{z}}$ is the regularization parameter determined via the Morozov's discrepancy principle [13].

It is noted that, given appropriate calibration or reference object, satisfactory shape reconstruction can be achieved [4], [5]. We don't deny that they are still promising technique, but the requirement of a priori information impedes a comparison between them and the proposed approach. In addition, as the computation of the proposed approach is straightforward, it is obviously more efficient than the deformable contour model proposed in [6].

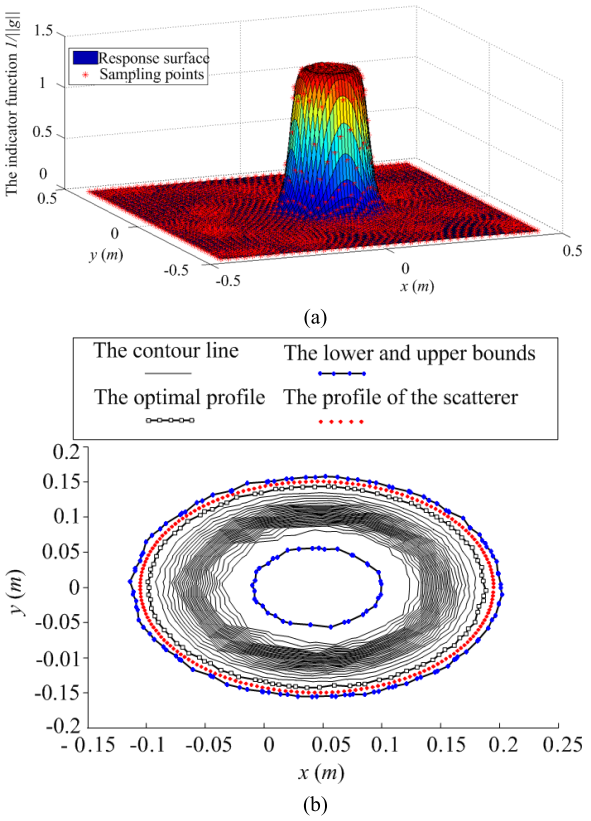

FIGURE 2. The case of a single scatterer; the response surface of the indicator function (a) and the contour plot of the indicator function, the lower and upper bounds, the optimal profile and the profile of the scatterer (b).

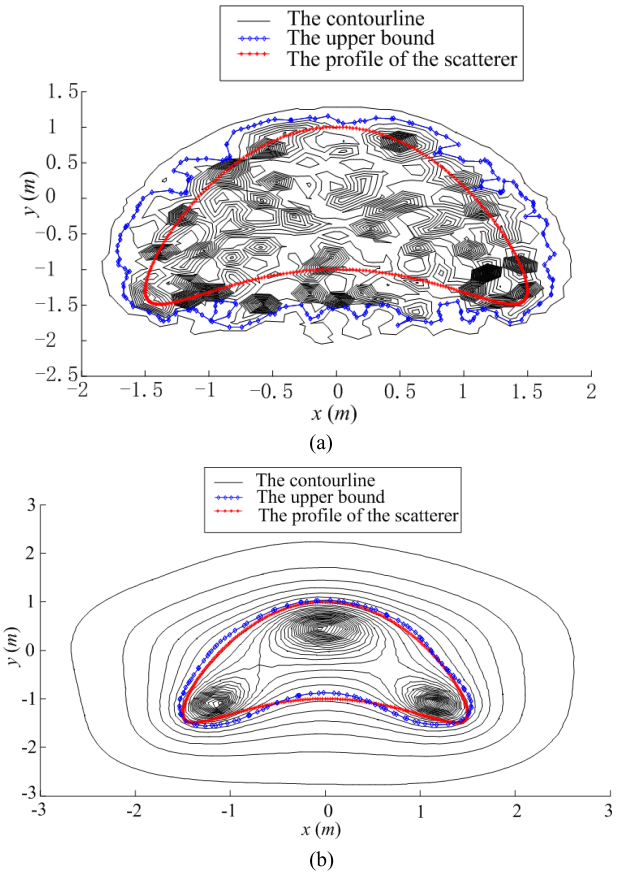

FIGURE 3. The recovered profile of the kite using different frequency of the incident wave: (a) the initial frequency 0.5 GHz, (b) the revised frequency 23 MH.

B. CASE STUDY: IMPENETRABLE CYLINDER

For the first case study, a single impenetrable cylinder is chosen as the scatterer. The response surface of the indicator function is demonstrated in Fig. 2. (*a*). The original profile is compared with the optimal profile in Fig. 2. (*b*), where the lower and upper bounds are also included. It is shown that the upper bound agrees with the predefined profile fairly well.

C. CASE STUDY: KITE

The second case study, besides the validation of the geometric feature analysis again, demonstrates the validation of the frequency bound deduced in (17). The famous scatterer "Kite" is used. As for the other assumptions, they are the same as the first case study. As the initial frequency is 0.5 GHz, which is very high, the recovered profile, as illustrated in Fig. 3 (*a*), becomes oscillatory. For every sampling point inside the identified profile (it is simply assumed as the upper bound), the corresponding residuals are different. In order to estimate the appropriate frequency limit of the incident wave using (17), some numerical experiments are conducted. It is found that the average residual of the sampling points inside the recovered profile is promising. The result is around 23 MHz. The revised recovered profile, as shown in Fig. 3(*b*), outperforms the initial one significantly. Further estimation provides higher frequency limit than 23 MHz (295 MHz), therefore, no more correction of the frequency is needed. The revised recovered profile, as shown in Fig. 3(b), outperforms the initial one significantly.

VI. CONCLUSION

This paper presents a parameter-free LSM. On the one hand, the cut-off value of the indicator function used in the edge detection could be extracted without parameters. On the other hand, the satisfying posterior estimation of the upper frequency limit of the incident electromagnetic wave is determined via the residual norms of the far-field equation. This proposed method can be extended to three-dimensional cases, which is left for future work.

REFERENCES

[1] W. Chew, *Waves and Fields in Inhomogeneous Media*, 1st ed. Piscataway, NJ, USA: Wiley, 1995, pp. 548–554.

[2] D. Colton and R. Kress, *Inverse Acoustic and Electromagnetic Scattering Theory*, 2nd ed. Berlin, Germany: Springer-Verlag, 1998.

[3] D. Colton and A. Kirsch, "A simple method for solving inverse scattering problems in the resonance region," *Inverse Problems*, vol. 12, no. 4, pp. 383–393, 1996.

[4] D. Colton, K. Giebermann, and P. Monk, "A regularized sampling method for solving three-dimensional inverse scattering problems," *SIAM J. Sci. Comput.*, vol. 21, no. 6, pp. 2316–2330, 2000.

[5] J. Li, H. Liu, and J. Zou, "Strengthened linear sampling method with a reference ball," *SIMA J. Sci. Comput.*, vol. 31, no. 6, pp. 4013–4040, 2010.
[6] R. Aramini, M. Brignone, J. Coyle, and M. Piana, "Postprocessing of the linear sampling method by means of deformable models," *SIAM J. Sci. Comput.*, vol. 30, no. 5, pp. 2613–2634, 2008.
[7] G. H. Li, X. Zhao, and K. M. Huang, "Frequency dependence of image reconstruction of linear sampling method in electromagnetic inverse scattering," in *Proc. Progr. Electromagn. Res. Symp.*, Xi'an, China, 2010, pp. 611–614.
[8] A. Roberts, "Curvature attributes and their application to 3D interpreted horizons," *First break*, vol. 19, no. 2, pp. 85–100, 2001.
[9] D. Levin, "The approximation power of moving least-squares," *Math. Comput. Amer. Math. Soc.*, vol. 67, no. 224, pp. 1517–1531, 1998.
[10] M. Alexa, *et al.*, "Point set surfaces," in *Proc. IEEE Vis.*, San Diego, CA, USA, Oct. 2001, pp. 21–28.
[11] F. G. Peet and T. S. Sahota, "Surface curvature as a measure of image texture," *IEEE Trans. Patten Anal. Mach. Intell.*, vol. 7, no. 6, pp. 734–738, Jun. 1985.
[12] R. Aramini, G. Caviglia, A. Massa, and M. Piana, "The linear sampling method and energy conservation," *Inverse Problems*, vol. 26, no. 5, 2010, Art. no. 055004.
[13] D. Colton, M. Piana, and R. Potthast, "A simple method using Morozov's discrepancy principle for solving inverse scattering problems," *Inverse Problems*, vol. 13, no. 6, pp. 1477–1493, 1997.

LEI LIU received the B.S. and M.S. degrees from the Hefei University of Technology, in 2004 and 2007, respectively, and the D.Eng. degree from Zhejiang University, Hangzhou, China, in 2012, all in electrical engineering, where he has been a Lecturer with the College of Electrical Engineering, since 2017.

From 2014 to 2016, he was a Research Associate with the Department of Electrical Engineering, The Hong Kong Polytechnic University. His research interests include inverse problems in electromagnetics and magnetic hysteresis modeling.

GUANZHONG HU received the B.S. degree in electrical engineering from Zhengzhou University, in 2003, and the M.S. and D.Eng. degrees from Zhejiang University, Hangzhou, China, in 2006 and 2016, respectively.

Since 2018, he has been a Lecturer with the School of Electrical Engineering and Mechano-Electronic Engineering, Xuchang University, Henan, China. His research interests include engineering optimization and bio-electromagnetics.